Design of High Efficiency Wound Field Synchronous Machine With Winding Connection Change Method

Myung-Seop Lim and Jung-Pyo Hong, *Senior Member, IEEE*

(Invited Paper)

***Abstract*—In this paper, a design method for a wound field synchronous motor (WFSM) employing the dual stator winding and the winding connection change circuit is proposed. Through the design method, the WFSM can be operated as two different modes, and each mode is determined by the connection between the stator windings U, V, W and X, Y, Z. By applying the proposed method to the conventional WFSM, the operation mode of the motor is changed at a certain speed. The speed for the mode change is determined to maximize the efficiency of the machine. As a result, through the mode change, the line to line induced voltage, current phase angle, and phase resistance are decreased. In addition, the demand field current is also reduced to achieve the required torque due to the salient pole characteristics of WFSM. Consequently, the efficiency of the WFSM is increased due to the mode change. Finally, the effect of the proposed method and the validity of the simulation results are verified by the load test.**

***Index Terms*—Dual stator winding, efficiency, induced voltage, magnetic torque, reluctance torque, salient pole, wound field synchronous machine (WFSM).**

I. Introduction

RECENTLY, electric motors are generally used in various industrial fields. There are various types of motors for industry applications, such as the induction motor (IM), synchronous reluctance motor (SynRM), surface-mounted permanent magnet synchronous motor (SPMSM), interior permanent magnet synchronous motor (IPMSM), wound field synchronous motor (WFSM), and so on. Among these, the rare-earth PM motors are typically used as they have a relatively high power density and can be applied to high-speed regions in the case of the IPMSM [1]–[4]. Thus, the rare-earth PM motor is the most commonly used motor at present [5]–[9]. However, rare-earth permanent magnets (PMs) have an unstable price as well as high cost. This has led to a variety of studies searching for alternative motor types with the same performance as the rare-earth PM motors but that do not require rare-earth PMs [10]. Among the rare-earth free motors, WFSM, which aside from not requiring rare-earth magnets, is advantageous to use in high-speed operations as it can effectively control the field current, apart from the flux weakening control, thereby eventually broadening the high-speed range and theoretically increasing the efficiency. Therefore, WFSM has a higher degree of freedom (DOF) for design and control methods than the other types of motors. In addition, WFSM is able to use both magnetic torque and reluctance torque through the vector control of the armature current. And so, WFSM achieves relatively higher torque than the other type of rare-earth free motors. Consequently, WFSM is used in a variety of industrial fields, including high speed applications such as traction and integrated starter and generator (ISG) of electric vehicle / hybrid electric vehicle (EV/HEV), despite the need for brush and slip-ring [11]–[13]. These are the reasons that WFSM is selected as the subject of study in this study.

A few academic papers discuss the design or control methods of WFSM to improve performance characteristics. Reference [14] and [15] describes the design method of the brushless WFSM to remove the brush and slip-ring which are the shortcomings of the conventional WFSM. Reference [16] discusses the optimum design method and control algorithm of WFSM to maximize efficiency. Reference [17]–[19] present design methods to improved torque characteristics of WFSM. In addition, reference [20] and [21] deal with control of WFSM using a z-source inverter to increase efficiency of the motor. Reference [22] discusses the control method of WFSM using both load commutator inverter and voltage source inverter to improve the controllability of the machine. However, the prior researches do not propose the methods to improve the efficiency as well as controllability at the same time. Furthermore, given the improvement of the efficiency and the operating point of the machine, the effectiveness of the proposed methods in the prior researches are not very significant to improve the efficiency and characteristics of WFSM.

In this paper, the background and characteristics of salient pole WFSM according to the phase angle of the input armature current are introduced, and the need for a new design method is explained. Based on this, a method of designing a WFSM employing series/parallel switching circuit, called a hybrid circuit (HC), WFSM is proposed. The method can improve the performance of WFSM in terms of its efficiency, reducing the induced voltage and *d*-axis current. First, the coil winding method that should be considered when designing the HC WFSM, and the

Manuscript received December 21, 2017; revised April 24, 2018; accepted June 6, 2018. Date of publication June 15, 2018; date of current version November 21, 2018. Paper no. TEC-00990-2017. *(Corresponding author: Jung-Pyo Hong.)*

M.-S. Lim is with the School of Mechanical Engineering, Yeungnam University, Gyeongsan 38541, South Korea (e-mail: limmang87@yu.ac.kr).

J.-P. Hong is with the Department of Automotive Engineering, Hanyang University, Seongdong-gu 04763, South Korea (e-mail: hongjp@hanyang.ac.kr).

Color versions of one or more of the figures in this paper are available online at http://ieeexplore.ieee.org.

Digital Object Identifier 10.1109/TEC.2018.2847728

connection method of each winding, are presented. Second, a simple switching circuit that makes it possible for the connections between the windings to be converted is also presented. Third, the determination method of the optimum speed condition for the circuit switching is described. As a result, through the proposed methods, the HC WFSM are designed. The characteristics of the HC WFSM are analyzed through the nonlinear finite-element method (FEM). Finally, the effectiveness and validity of the presented method are verified through experiments.

II. Characteristics and Issue of WFSM

WFSM has basic differences and characteristics compared to those of the permanent magnet synchronous machines (PMSMs) such as IPMSM and SPMSM. They are the controllability of the field flux by controlling the field current as well as the saliency based on the *d*, *q*-axis inductance. These characteristics of WFSM increase the degree of freedom (DOF) of the design and affect the performance of the machine in terms of torque, efficiency, induced voltage, and current phase angle. Therefore, the torque and induced voltage characteristics of WFSM are analyzed based on the basic equations. Furthermore, from the analysis results, the necessity of the new design method for WFSM to overcome the limitations and improve its performance is described.

A. General Characteristics of WFSM

The greatest difference between WFSM and the PMSMs is the controllability of the field flux. Field weakening on the PMSM is possible by applying a negative *d*-axis armature current. But as opposed to the PMSM, WFSM allows not only for applying a negative *d*-axis current, but for flux weakening, which reduces the field current (current to the pole winding) itself. While applying a negative *d*-axis current causes an increase of copper loss, reducing the field current causes a decrease of copper loss. Therefore, theoretically, a relatively efficient high speed operation is possible by applying the control method of reducing the field current more proactively. Since the field current affects the magnitude of the flux linkage, which in turn directly affects the performance of the WFSM, such as induced voltage and output torque, controlling the field current is crucial to operate the WFSM efficiently. Thus, WFSM has a higher DOF for design and control methods than PMSMs.

Another difference between WFSM and PMSM is the saliency or saliency ratio. Saliency ratio is the inductance ratio between the *d*- and *q*-axis. While both WFSM and IPMSM are salient pole machines, the difference is that in WFSM, the inductance on *d*-axis is greater than that on *q*-axis ($L_d > L_q$); in IPMSM, on the other hand, the inductance on *d*-axis is smaller than that on *q*-axis ($L_d < L_q$). Such salient pole machines can use both magnetic torque and reluctance torque. However, reluctance torque depends on not only the phase of the armature current, but saliency ratio ($L_d > L_q$ or $L_d < L_q$). Thus, the characteristics of WFSM and IPMSM are different.

As shown in Fig. 1(a) and (b), WFSM can be controlled with the 1st quadrant or 2nd quadrant operation based on the current phase angle. To analyze the torque and voltage characteristics

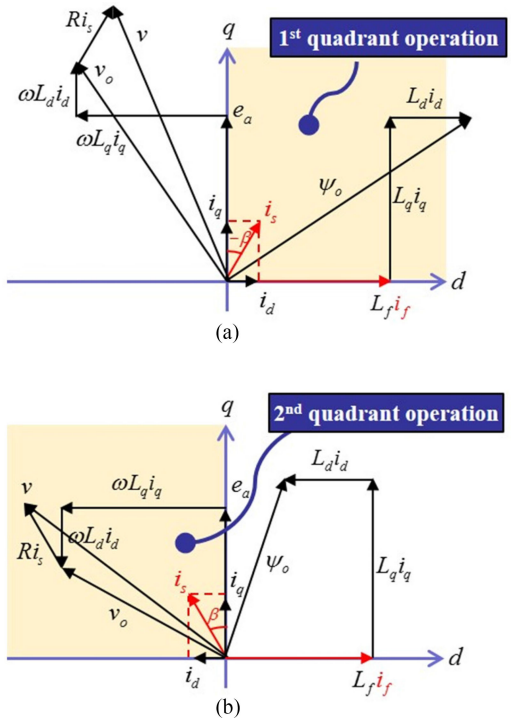

Fig. 1. Vector diagram of WFSM. (a) 1st quadrant operation. (b) 2nd quadrant operation.

of salient pole WFSM with $L_d > L_q$, thus, the current phase angle for both 1st and 2nd quadrant operations should be considered. Fig. 1 presents the vector diagrams of WFSM according to the current phase angle of the input armature current. i_s is the armature current and β is the current phase angle. i_d and i_q, are *d*, *q*-axis armature current. L_d and L_q are *d*, *q*-axis inductance, respectively. i_f and L_f are the field current and field inductance. v is the input voltage and v_o is the induced voltage. R is phase resistance, ψ_a is the no-load flux linkage, and ω is the rotational speed in the electrical angle. Iron loss is neglected for the diagrams.

B. Torque and Induced Voltage of WFSM

The torque and induced voltage characteristics of WFSM according to the current phase angle are examined based on the basic theory to understand the limitations of WFSM. Equation (1) and (2) shown below are the torque equation and the induced voltage equation of the armature circuit disregarding the phase resistance. Iron loss is neglected for the equations as well.

$$T = T_m + T_r = P_n \left[\left(L_f i_f i_a \cos\beta \right) + \frac{1}{2} \left(L_q - L_d \right) i_a^2 \sin 2\beta \right] \quad (1)$$

$$v_0 = \omega \sqrt{\left(L_d i_d + L_f i_f \right)^2 + \left(L_q i_q \right)^2} \quad (2)$$

The first term in the torque formula above is magnetic torque T_m, and the second term is reluctance torque T_r. P_n is number of pole pair. L_f and i_f are inductance and input current of rotor coil, respectively. i_a is input current of stator, and β is

TABLE I
TORQUE CHARACTERISTICS ACCORDING TO CURRENT PHASE

Torque	WFSM ($L_d > L_q$)	IPMSM ($L_d < L_q$)
1st quadrant operation ($-90^\circ<\beta<0^\circ$)	$+T_m$ $+T_r$	$+T_m$ $-T_r$
2nd quadrant operation ($0^\circ<\beta<90^\circ$)	$+T_m$ $-T_r$	$+T_m$ $+T_r$

TABLE II
VOLTAGE CHARACTERISTICS ACCORDING TO CURRENT PHASE

Voltage	d-axis flux	Induced voltage
1st quadrant operation ($-90^\circ<\beta<0^\circ$)	$+L_d i_{od}$ $+ L_f i_f$	Relatively high
2nd quadrant operation ($0^\circ<\beta<90^\circ$)	$-L_d i_{od}$ $+ L_f i_f$	Relatively low

the current phase angle. v_o is the induced voltage, and ω is the rotational speed in the electrical angle. i_d and i_q, are d, q-axis armature current. L_d and L_q are d, q-axis inductance, respectively. The output torque of WFSM is generated by the sum of two components. Based on the equations, the torque and voltage characteristics of WFSM are analyzed in this paper.

Table I shows the relations between T_m and T_r when the ideal WFSM is controlled in the 1st quadrant ($-90^\circ < \beta < 0^\circ$) and the 2nd quadrant ($0^\circ < \beta < 90^\circ$), for the analysis of the torque and voltage characteristics according to the phase of the armature current. As shown in Table I, when WFSM is controlled in the 1st quadrant, the signs of the magnetic and reluctance torques are equal. When WFSM is controlled in the 2nd quadrant, however, the signs of the magnetic and reluctance torques are different. Therefore, total output torque which is sum of the magnetic and reluctance torques is decreased.

Table II shows the d-axis flux and induced voltage characteristics when WFSM is controlled in the 1st quadrant ($-90^\circ <\beta <0^\circ$) and the 2nd quadrant ($0^\circ <\beta < 90^\circ$). As shown in Table II, when WFSM is controlled in the 1st quadrant, the signs of the d-axis flux by the armature current and the d-axis flux by the field current are equal, and as such, the induced voltage becomes very high. When WFSM is controlled in the 2nd quadrant, however, the signs of the two fluxes become opposite from each other, and the induced voltage is offset and becomes smaller.

The higher the speed of a motor is, the greater the induced voltage, which in turn causes voltage saturation. Accordingly, the induced voltage should be reduced so as to extend the driving speed of the motor, and as shown in Table II, driving in the 2nd quadrant is required. As shown in Table I, however, when WFSM drives in the 2nd quadrant, the signs of the magnetic and reluctance torques become opposite from each other, and the total torque is reduced. Consequently, the input field and armature currents increases to achieve the targeted torque and power, which in turn increases the voltage. These are the fundamental characteristics of the torque of WFSM. When driving at high speed, the input current and induced voltage increase to achieve target torque and power, which deteriorates the controllability of the motor, and the efficiency declines.

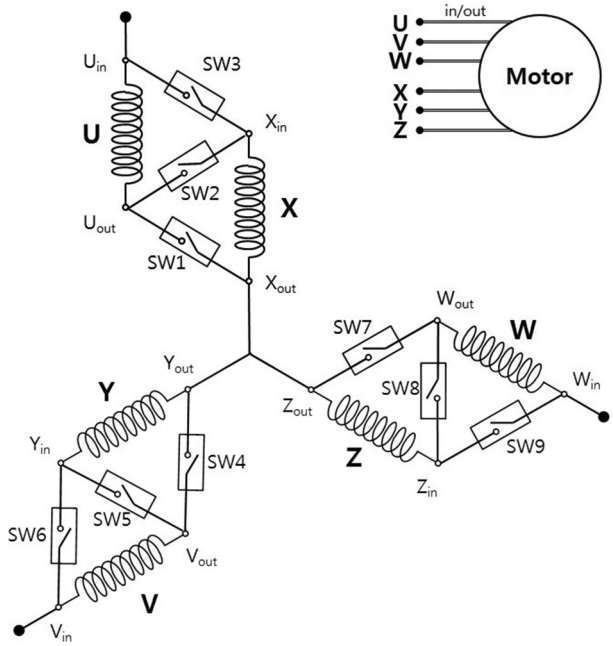

Fig. 2. The schematic diagram of the armature windings for the proposed method.

III. PROPOSED METHOD: HYBRID CIRCUIT (HC) WFSM

In this paper, the design method for WFSM using a series/parallel switching circuit of armature windings is proposed from the engineering perspective to overcome the weakness of WFSM as described in Section II-B. Through the proposed method, the series turn per phase, inductance, and phase resistance can be changed at a certain speed range. As a result, the induced voltage and d-axis current can be reduced as well as improving the efficiency of the machine. In addition, in this paper, the determination method of the optimum speed for the circuit switching is proposed to maximize the efficiency of WFSM.

A. Design of HC WFSM

The windings of each phase are divided into winding 1 and winding 2, and both windings are wound on the same teeth of a stator as dual winding. Winding 1 consists of U, V, and W. Winding 2 consists of X, Y, and Z in this paper. The schematic diagram of the stator for the three-phase HC WFSM and switching table for each mode are shown in Fig. 2 and Table III, respectively. The motor and the inverter are connected to the switching circuit, and the on/off control of the switch changes the winding circuit. As shown in Fig. 2, the required number of on/off switching elements for using both series and parallel modes is three. These are the minimum numbers of the required elements because the additional safety circuits or additional algorithm considering any sudden variation of the voltage and current in transient state during mode change are neglected in this paper.

TABLE III
SWITCHING TABLE OF HC WFSM

Winding1: U, V, W Winding2: X, Y, Z	Switch number (SW)	Series mode	Parallel mode
A phase: U, X	SW 1	Off	On
	SW 2	On	Off
	SW 3	Off	On
B phase: V, Y	SW 4	Off	On
	SW 5	On	Off
	SW 6	Off	On
C phase: W, Z	SW 7	Off	On
	SW 8	On	Off
	SW 9	Off	On

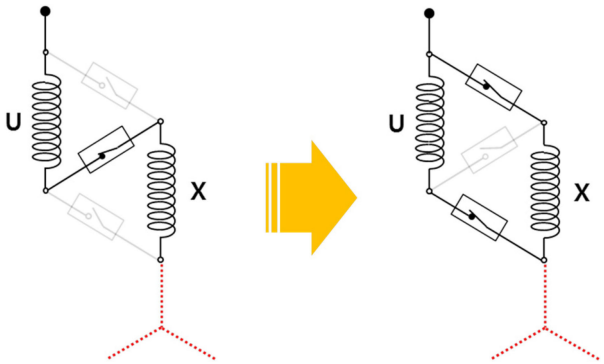

Fig. 3. Hybrid circuit; Series mode to parallel mode.

As a simple method of the control for the mode change, the input power of the inverter can be temporarily turned off when changing the mode at a specific condition, and the power is turned on after changing the winding circuit with the switching. Indeed, the power on/off and switching should be performed as fast as possible. If the inverter is switched off and on in a very short time by the control algorithm or simple safety circuit, this method is a relatively easy solution. On the other hand, a sudden change of the circuit during the operation (with the inverter continuously switched on) will cause a huge surge in the voltage or current. Therefore, mode change during the operation is possible with the additional protection circuit or control algorithm in order to protect the controller and inverter from a surge in voltage or current.

The connections of the windings are converted to series and parallel modes through a change in the circuits using switches. Fig. 3 presents the schematic diagrams of the one phase for series and parallel modes. Each phase consists of two parts of windings such as U&X, V&Y, and W&Z, respectively. Thus, when the series mode is changed to the parallel mode, the series turn number per phase becomes 1/2, and the armature phase resistance becomes 1/4. Consequently, the induced voltage and current phase angle are decreased. Thus, the *d*-axis input current can be decreased. In addition, the input field current to achieve the required torque can be reduced for WFSM due to the decrease of the negative reluctance torque As a result, it is expected that the efficiency of the motor is increased, even though the *q*-axis input current is increased to fulfill the required torque.

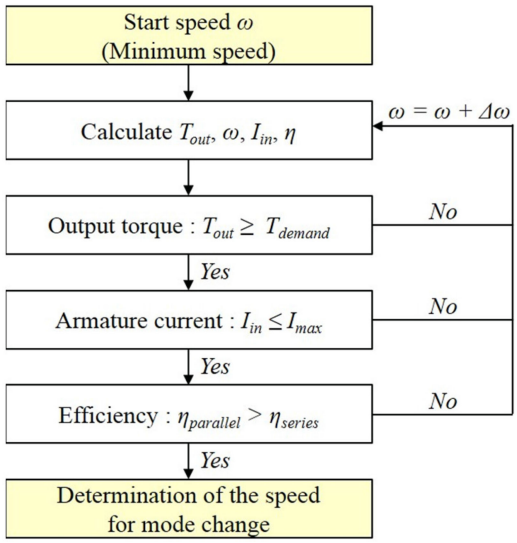

Fig. 4. Determination process for the mode change.

Through the proposed method, the series turn number per phase of the motor can be changed appropriately according to the operating speeds. The motor is operated at a low/middle speed as the series turn per phase is *N*. On the other hand, the motor can be operated as the series turn per phase is *N*/2 after changing the winding connection at a certain speed. In this paper, such a motor/controller system is called a "hybrid circuit (HC) machine."

B. Determination of Speed for Mode Change

The series mode can be changed to a parallel mode at a certain speed to achieve the reasonable torque proportion as well as increasing the efficiency of WFSM. These are the main effects of the HC method. These are the results from not only a decrease of the current phase angle which is related to the controllability, but also a decrease of the armature resistance. When the mode is changed, the induced voltage, field current, *d*-axis armature current, and phase resistance are decreased. However, *q*-axis armature current is increased to fulfill the required torque due to the decrease of flux linkage. Therefore, the output torque, input current, and efficiency are considered to determine the optimum speed for mode change. Fig. 4 presents the determination process of the mode change speed considering the required performance and efficiency. Conclusively, the speed for mode change can be determined when HC WFSM is fulfilling the following conditions simultaneously: the required torque is achieved, the input current does not exceed the current limit, and the efficiency is increased comparing to that of the series mode.

IV. CHARACTERISTICS OF HC WFSM

The analysis model is proposed and applied to the HC method. The configuration and specifications of the model are shown in Fig. 5 and Table IV, respectively. The effect of the HC method on the performance of the motor is simulated and verified herein by analyzing the efficiency as well as the performance curve of

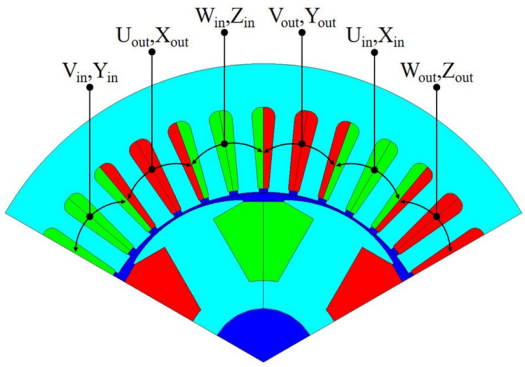

Fig. 5. Configuration of the analysis model.

TABLE IV
SPECIFICATIONS OF HC WFSM

	Unit	Value
Pole / Slot	-	6 / 36
Stack length	mm	60
Air-gap length	mm	0.5
Outer diameter	mm	128
Series turn / phase (armature coil)	-	48
Parallel number (armature coil)	-	1
Turn / pole (field coil)	-	300
DC voltage	V	115
Current limit	A_{rms}	60
Max. torque	Nm	20
Rated speed	rpm	2000
Rated power	kW	4.2
Max. speed	rpm	7000

the torque, speed, and current of the proposed model by means of nonlinear FEM. To analyze the electromagnetic field, this study used E.M.F (version 2.2), a program that our laboratory developed. This software, similar to MAXWELL or JMAG in its functionality, is currently being used by many companies in South Korea.

To derive the most accurate simulation result, all potential losses were considered. Not only the copper loss in the windings of the stator and rotor of the WFSM, but the resistance of the wire connected from the inverter to the motor were measured and considered to the simulation. For the core loss, the loss test results of the core material, which was actually used in the production, was used in conducting the FEM. The flux density of each element was derived from the nonlinear analysis results, and the losses based on the flux density and frequency at each element were obtained from the material test results for the calculation [9]. Additionally, after connecting the motor to the dynamo set, the mechanical loss in the test motor was considered to the simulation through the mechanical loss test, in other words, the no-load test.

A. Characteristics Curve

The motor performance, such as the torque, speed, and current, according to each mode is analyzed through the WFSM theory and the maximum efficiency control method [16]. Mechanical loss is obtained by the no-load test and the result is considered to simulate the characteristics and performance of WFSM.

As has been mentioned in Section II-B, for WFSM to reduce the induced voltage at high speed, it performs flux weakening control that lowers the field current. But, lowering the field current causes the reduction of the flux linkage. Thus, to achieve the target torque, the input armature current must be increased, at which, the target torque may not be achieved in some occasions due to the limitation of the armature current. Consequently, the WFSM in the maximum efficiency control decreases the field current slightly and performs the 2nd quadrant operation that applies a negative current on d-axis. However, as opposed to IPMSM, the WFSM in the 2nd quadrant operation generates a negative reluctance torque, which is in opposite direction to the magnetic torque. The WFSM with $L_d > L_q$ in the 2nd quadrant operation cannot generate a positive reluctance torque. Instead, the method proposed by this paper is to acquire the margin of the induced voltage by changing the connection of the armature winding at high speed and to make the negative reluctance torque almost zero by minimizing the magnitude of the current on d-axis. As a result, the reduction of the negative reluctance torque results not only in the input armature current for achieving the target torque, but in the reduction of the field current, which, as a consequence, leads to the very efficient high speed operation. Since the reluctance torque of the WFSM in the 2nd quadrant operation is in opposite direction of the magnetic torque, it is best to lower its magnitude down to 0 or operate in the 1st quadrant operation to achieve the required torque.

Fig. 6(a) shows the characteristic curve when the proposed WFSM is controlled with the maximum efficiency algorithm. In Fig. 6, [Arms] in the left y-axis is root mean square value of the input current, and 'Arm. Current' of the purple line with the star symbol means armature current. The series turn per phase of the proposed motor was originally designed as 48. Thus, it can be considered a series mode because the series turn per phase is 48 by the series connection between winding 1 and winding 2. Fig. 6(b) shows the variations in characteristics when the mode is changed. It shows the characteristic curve when the series mode is changed to the parallel mode. In such a case, the mode is changed at 4000 rpm, and thus, the armature current supplied to the motor does not exceed 60 A_{rms}, which is the limitation of input current. As a result, the line to line induced voltage is decreased by 23.95 V at maximum by the mode change. The current phase angle of the armature current is decreased from 59.76 degrees to -2.45 degrees at maximum. This results shows that the current phase of the WFSM is changed from the 2nd quadrant to the 1st quadrant by the HC method. The field current is also reduced from 2.49 A to 1.56 A at maximum.

The examination of the results of the mode change revealed that the current phase angle is reduced, and the field current also decreases, which is caused by the reduction of the induced voltage by the mode change. Therefore, the required magnetic torque can be decreased fulfilling the demand torque by reducing the negative reluctance torque as shown in Fig. 7. It seems that the reductions of the phase angle of the armature current and the d-axis current as well as armature phase resistance lead

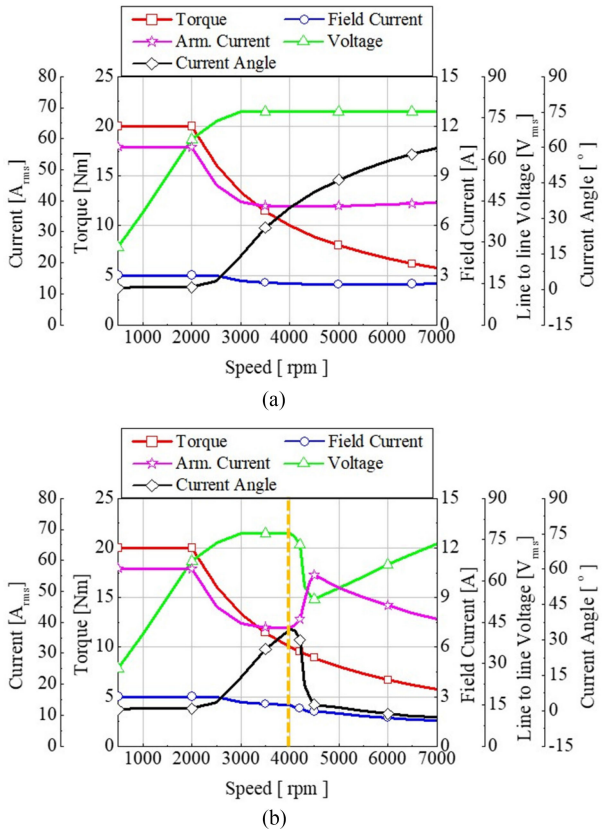

Fig. 6. Characteristic curves of the analysis model. (a) Originally designed WFSM; Series mode. (b) WFSM applied HC method; Series mode to parallel mode.

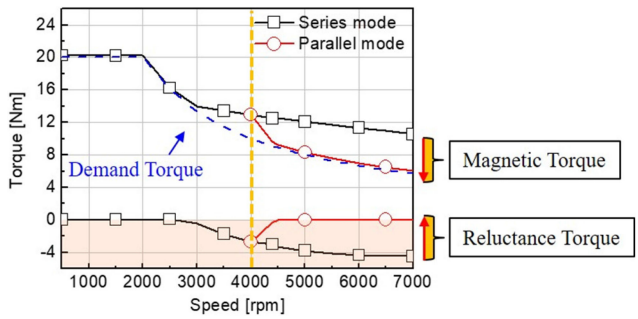

Fig. 7. Proportions of the output torque according to each mode.

to motor efficiency improvement even though the q-axis current is increased as shown in Fig. 8.

B. Efficiency Map

The proposed design method for WFSM consequently leads to the improvement of the efficiency of the machine. Therefore, an efficiency map of the proposed WFSM should be examined. Efficiency η of the WFSM is calculated by (3) as shown below.

$$\eta = \frac{P_{\text{out}}}{P_{\text{in}}} = \frac{T\omega}{T\omega + P_{\text{Total loss}}} \tag{3}$$

where T is the output torque and ω is rotational speed. P_{out} and P_{in} are output power and input power, respectively. $P_{Total\,loss}$ is the sum of the motor losses such as armature copper loss, field

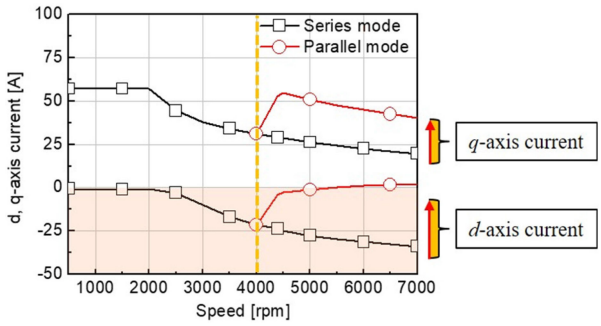

Fig. 8. Proportions of the armature current according to each mode.

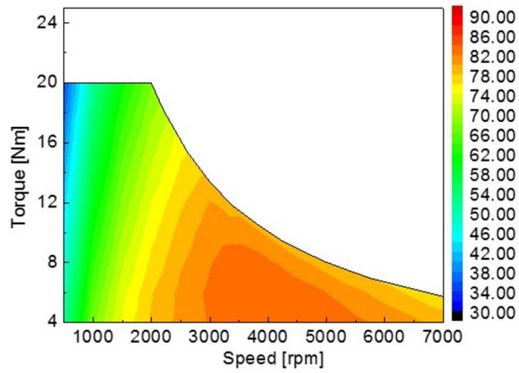

Fig. 9. Efficiency map of conventional WFSM (series mode).

copper loss, core loss, and mechanical loss. When simulating the motor efficiency by using (3), copper loss and iron loss were estimated through the analytical method and nonlinear FEM, respectively. The mechanical loss was measured with a test by using a prototype, the result of which was considered in the equation. The mechanical loss was calculated by measuring the speed and torque when the test motor (prototype) is driven by the load motor under the no-load conditions. Fig. 9 shows the result of the maximum efficiency control when the motor proposed in this paper is in series mode. Fig. 10 shows the efficiency when the motor is changed to the parallel mode from 4000 rpm. Compared to the efficiency of the series mode in the high speed region, the efficiency of the parallel mode improved by up to 12%. This is because not only does the magnitude of the field current and d-axis current input for field weakening or flux weakening decrease, but also the magnitude of the armature coil resistance, thereby resulting in a huge reduction of the copper loss as shown in Fig. 11(a) and (b). This causes an increase in efficiency after the mode change at 4000 rpm. The data shown in the figures present the copper losses under the conditions of the maximum power at 4500 rpm and 7000 rpm, respectively. As for the iron loss, the level or area of the partially magnetic saturation are varied nonlinearly depending on the specifications of the model including its shape, material and the load conditions (magnitude and phase angle of the armature current). In fact, the simulation in which the proposed method was applied to various types of motors showed that the iron loss of some models increases, while the iron loss of the others decreases. However, we identified a considerable decrease in copper loss of all models

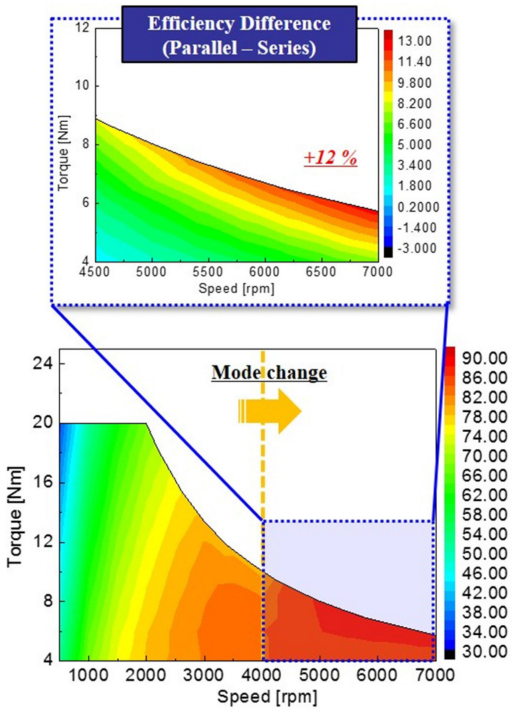

Fig. 10. Efficiency map of HC WFSM and efficiency difference between the modes.

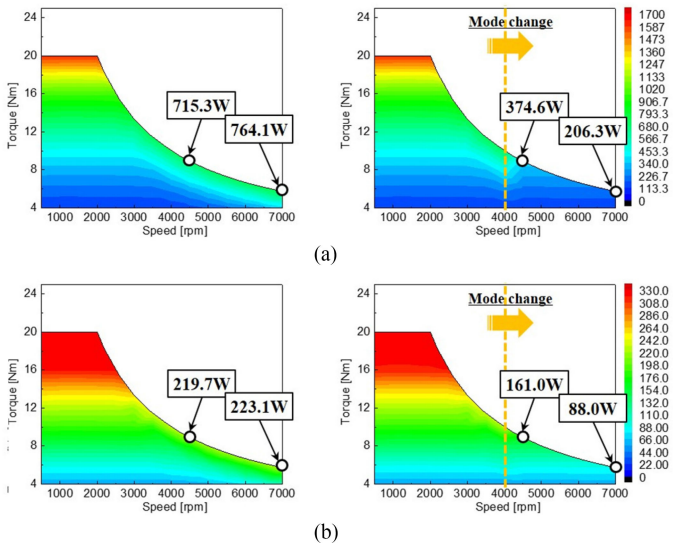

Fig. 11. Comparison of copper loss map. (a) Armature copper loss (left: conventional WFSM, right: HC WFSM). (b) Field copper loss (left: conventional WFSM, right: HC WFSM).

that were analyzed. Since the magnitude or the decrease ratio of copper loss is considerably larger than that of the iron loss, the efficiency of analyzed models ended up being improved considerably. The model applied in this study showed some increase of iron loss depending on the mode change as shown in Fig. 12. The data shown in the figures present the iron losses under the conditions of the maximum power at 4500 rpm and 7000 rpm, respectively. However, in the WFSM proposed in the

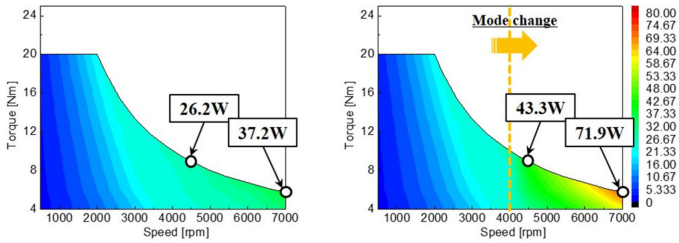

Fig. 12. Comparison of iron loss map (left: conventional WFSM, right: HC WFSM).

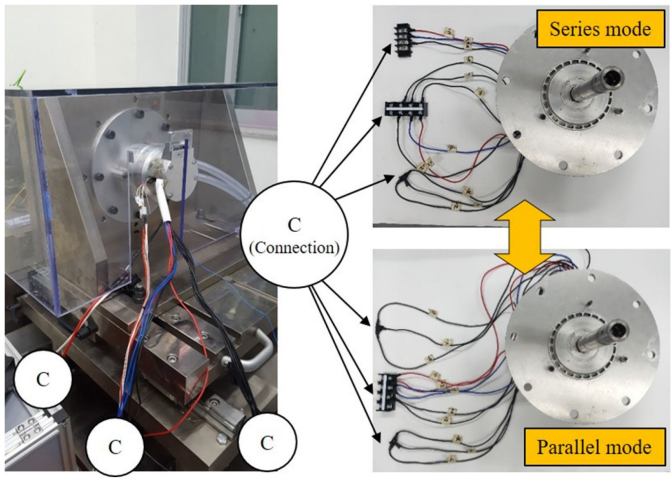

Fig. 13. Connections of the HC WFSM.

study, the overall efficiency was largely affected by the decrease in copper loss and it has remarkably improved.

V. Experimental Verifications

A load test is conducted to verify the characteristics of the test motor and effectiveness of the proposed method. In this study, the load test for each mode is conducted independently. When producing WFSM for this study, we made sure that each line of X, Y, Z, U, V, and W is not connected inside the motor housing, but the ends of these lines are out from the motor housing. Then, these lines are connected to the terminal block, through which all lines are connected outside the motor as shown in Fig. 13. In the actual experiment for the mode change, the motor operated in a series mode for up to 4000 rpm, and after stopping the motor, the mode was changed to the parallel mode by directly changing the connection manually between the X, Y, Z, U, V, and W on the terminal block. After changing the connection, we ran the test in parallel mode at the speed over 4000 rpm. In other words, the mode change, that is, the circuit change, was not made through commands of the controller or automatically, but made manually in this study.

The load test requires a driver, controller, dynamometer, power analyzer, oscilloscope, etc. The actual set-up for the test is shown in Fig. 14. For the test, the test motor is operated by the torque control and the load motor is operated by the speed control. The magnitude and phase angle of the current estimated by the simulation in Fig. 6 were applied as the reference values

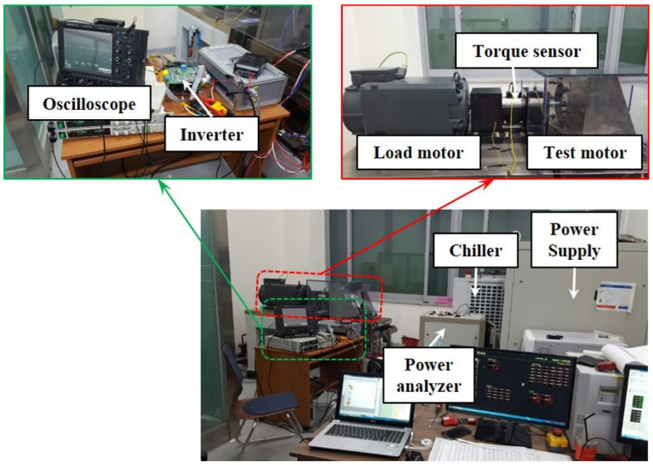

Fig. 14. Set-up for the load test.

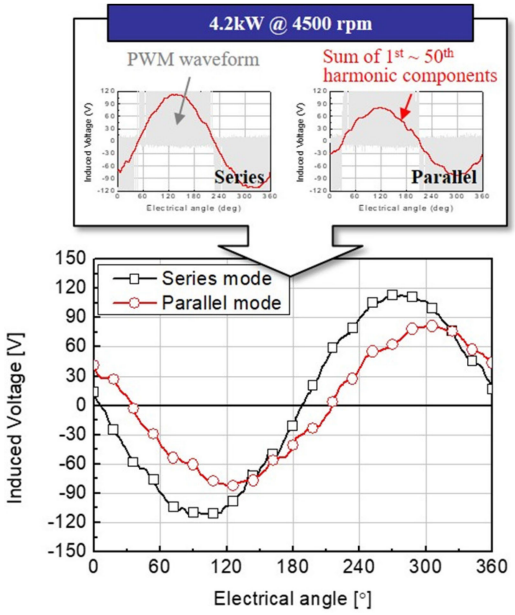

Fig. 15. Line to line induced voltage obtained from the load test.

of the controller. Actual input voltage and current are measured by using voltage and current probes, and input power is calculated through the power analyzer. Output power is calculated by measuring the torque and rotational speed. In order to compare the characteristics obtained from the simulation and experiment results, we try to maintain a 40 °C operating temperature during the load test, because copper temperature affects loss, which affects efficiency of the machine. The test was conducted while the motor was water-cooled with a chiller, observing the temperature with a temperature sensor installed on the coil. When it went below 40 °C, the data were measured after increasing the coil temperature to 40 °C by running the motor continuously. On the other hand, if the coil temperature exceeded 40 °C, the motor was temporarily suspended or ran at low input current to reduce the temperature to 40 °C and the data were measured. As a result, the study was able to measure the data at 40 °C in all operation points, and a large amount of time was spent on conducting the test at the exact temperature condition.

A. *Characteristic Curve*

The induced voltage is important because it affects the operating point of the salient pole WFSM. If the induced voltage is not saturated, WFSM can be operated at the 1st quadrant in *d*, *q*-axis. As a result, WFSM can be operated efficiently as described in Section II. Fig. 15 presents the line to line induced voltage waveform under the maximum load condition at 4500 rpm right after the mode change. It is very difficult to directly measure the induced voltage during the load test. In this study, the pulse width modulation (PWM) voltage, which was used each for the series mode and parallel mode under the same torque and speed conditions, was measured experimentally in order to compare, even indirectly, the magnitude of the induced voltage under the load condition at each mode. In addition, after conducting the analysis of the harmonics of the measured PWM waveforms by using the Fourier transform, the induced voltage waveforms under the load condition were obtained and compared by adding waveforms from the fundamental component to the 50th harmonic components. It is generally correct that the magnitude of the induced voltage generated by the field flux is related to the series turn number, with two times the difference. However, the field flux should be constant under a no-load condition, thus indicating that the armature input current should be 0. Fig. 15 shows the induced voltage waveform under load condition (armature current is applied in flux weakening region), at which the magnitude and phase of the armature current in the series mode are very different from those in the parallel mode. Moreover, the magnitude of the field flux is different at each mode because the magnitude of the field current at each mode is also different. Therefore, the voltage waveform under the load condition induced by the combined flux waveform of the field flux and the armature flux may show a phase that differs by each mode, and the difference in magnitude may not exactly be two times. As a result, it was found that when the motor operated in parallel mode, the magnitude of the line to line induced voltage showed greater reduction compared with the case in which the motor operated in series mode as expected. It was verified that the magnitude of the line to line induced voltage decreased due to the mode changes by the proposed method. Therefore, it infers that the reduction of the induced voltage leading to the 1st quadrant operation of WFSM, and this demonstrates that the machine operated efficiently by optimum controlling of the armature and field currents. The characteristic curve of the HC WFSM is shown in Fig. 16 as the test results. In Fig. 16, [Arms] in the left y-axis is root mean square value of the input current, and 'Arm. Current' of the purple line with the star symbol means armature current. Fig. 16 shows the actual current, voltage, and torque measured. The errors may not be notable, so that Figs. 6(b) and 16 may not look different. Due to the tendency in which the change in parameters is similar to each other, it would not be easy to compare the two figures. However, they are two different graphs, wherein the former shows the simulation results, and the latter shows the experimental results. Especially, the comparison of the values on the voltage line (the green line

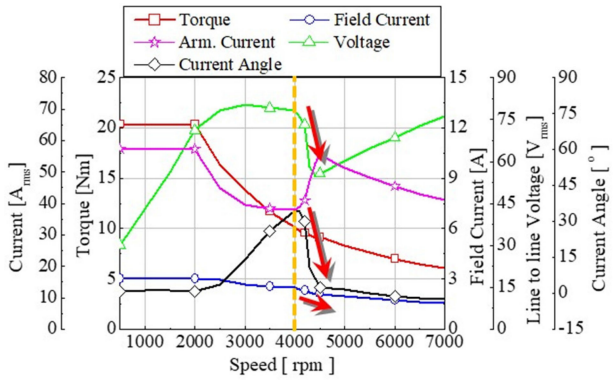

Fig. 16. Characteristic curve of the HC WFSM.

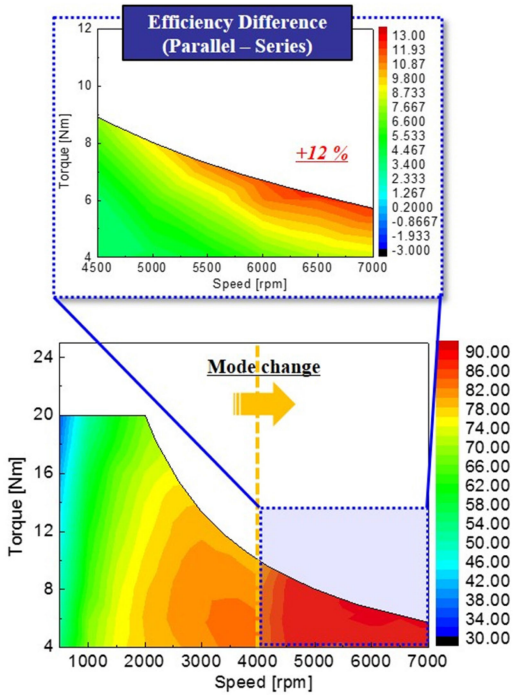

Fig. 17. Efficiency map of the HC WFSM as the test result.

with triangle symbols) shows that while the tendency is very similar, these values are somewhat different. For example, line to line induced voltages as the simulation results at 4500 rpm and 7000 rpm in Fig. 6(b) are 53.3 V and 73.7 V, respectively. However, the induced voltages as the test results at 4500 rpm and 7000 rpm in Fig. 16 are 55.8 V and 76.2 V, respectively. Consequently, it is concluded that the estimated characteristics of the test motor as presented in Section IV-A are almost the same as those of the test result.

B. Efficiency Map

Fig. 17 presents the efficiency maps of the HC WFSM as per the test results. The output power was divided by the input power to evaluate the efficiency. At this point, the output power was calculated by measuring the output torque and speed, and the input power was derived by measuring the input voltage and current, and the power factor. The mode of the motor is

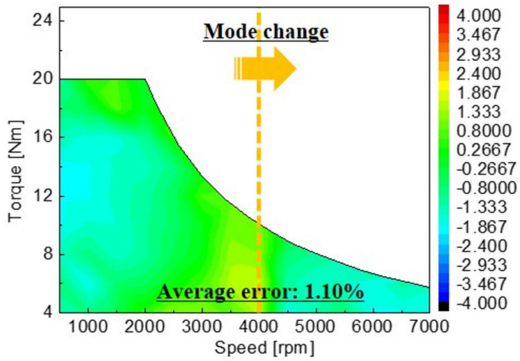

Fig. 18. Error of efficiency between simulation and test results.

changed from the series mode to parallel mode at 4000 rpm. The efficiency error of the HC WFSM between the simulation and experiment results is shown in Fig. 18. The average of the absolute value of the error is just 1.10%. The maximum error between the simulation and experiment results is about $\pm 1.88\%$. Given such results, the validity of the simulation results shown in Fig. 10 is verified. Therefore, it is concluded that the efficiency of the HC WFSM at middle and high speed region is largely improved through the proposed method.

For the HC system, it is expected that there are additional losses at the switching circuit for the mode change. However, from the perspective of the motor/inverter system, the copper loss at the motor is more dominant than the additional switching loss at the switching circuit. Furthermore, the switch added in this study operates only when there is a mode change. Since the effect of the copper loss reduction at the motor is considerably larger than that of the additional loss at the switch, the proposed system can be more advantageous in terms of efficiency. In addition to improving the efficiency of the machine, the method proposed reduces the phase angle of the input armature current, making it easier to control high speed operation in flux weakening region.

VI. Conclusion and Further Work

In this paper, the limitation of WFSM which can be operated in the 1st quadrant as well as the 2nd quadrant through the current vector control is analyzed. To overcome the weakness, a design method adopting a dual winding and series/parallel switching method is proposed. Through the proposed method, WFSM can be operated as series and parallel modes. Each mode refers to the connection between winding1 and winding2 of the dual stator winding. By applying the method to the proposed WFSM, it can be operated as a series mode until 4000 rpm and as a parallel mode after 4000 rpm. As the results show, line to line induced voltage is decreased by 23.95 V at maximum by the mode change. The current phase angle of the armature current is decreased from 59.76 degrees to -2.45 degrees at maximum. It shows that the input current phase is changed from the 2nd quadrant to the 1st quadrant region by the mode change. In addition, the field current is also reduced from 2.49A to 1.56A at maximum. Consequently, the speed range operated in the 1st quadrant is greatly extended, and the efficiency of

the motor is increased by 12% at maximum. Finally, the effect of the proposed method and reliability of the simulation results are verified by the load test. However, in this paper, the cost and switching loss by adding the switch to the control system is not discussed. In addition, the control method for the automatic mode change and the safety circuit considering sudden variations of the circuit parameters during the operation are not presented. Therefore, in the future, the controller system for HC WFSM will be researched based on the effectiveness of the proposed method and system.

REFERENCES

[1] E. Odvarka, A. Mebarki, D. Gerada, N. Brown, and C. Ondrusek, "Electric motor-generator for a hybrid electric vehicle," *Eng. Mech.*, vol. 16, no. 2, pp. 131–139, 2009.

[2] M. Zeraoulia, M. E. H. Benbouzid, and D. Diallo, "Electric motor drive selection issues for HEV propulsion systems: A comparative study," *IEEE Trans. Veh. Technol.*, vol. 55, no. 6, pp. 1756–1764, Nov. 2006.

[3] M. J. Melfi, S. Evon, and R. McElveen, "Induction versus permanent magnet motors," *IEEE Ind. Appl. Mag.*, vol. 15, no. 9, pp. 28–35, Nov./Dec. 2009.

[4] A. J. Grobler, S. R. Holm, and G. van Schoor, "A two-dimensional analytic thermal model for a high-speed PMSM magnet," *IEEE Ind. Electron.*, vol. 62, no. 11, pp. 6756–6764, Nov. 2015.

[5] J. Y. Lee, S. H. Lee, G. H. Lee, J. P. Hong, and J. Hur, "Determination of parameters considering magnetic nonlinearity in an interior permanent magnet synchronous motor," *IEEE Trans. Magn.*, vol. 42, no. 4, pp. 1303–1306, Apr. 2006.

[6] K. T. Kim, K. S. Kim, S. M. Hwang, T. J. Kim, and Y. H. Jung, "Comparison of magnetic forces for IPM and SPM motor with rotor eccentricity," *IEEE Trans. Magn.*, vol. 37, no. 5, pp. 3448–3451, Sep. 2001.

[7] J. Hur and B. W. Kim, "Rotor shape design of an interior PM type BLDC motor for improving mechanical vibration and EMI characteristics," *J. Elect. Eng. Technol.*, vol. 5, no. 3, pp. 462–467, Sep. 2010.

[8] G. Wang, L. Yang, B. Yuan, B. Wang, G. Zhang, and D. Xu, "Pseudo-random high-frequency square-wave voltage injection based sensorless control of IPMSM drives for audible noise reduction," *IEEE Trans. Ind. Electron.*, vol. 63, no. 12, pp. 7423–7433, Dec. 2016.

[9] M. S. Lim, S. H. Chai, J. S. Yang, and J. P. Hong, "Design and verification of 150-krpm PMSM based on experimental results of prototype," *IEEE Trans. Ind. Electron.*, vol. 62, no. 12, pp. 7827–7836, Dec. 2015.

[10] I. Petrov, M. Niemela, P. Ponomarev, and J. Pyrhonen, "Rotor surface ferrite permanent magnets in electrical machines: advantages and limitations," *IEEE Trans. Ind. Electron.*, vol. 64, no. 7, pp. 5314–5322, Jul. 2017.

[11] H. Liu, L. Xu, M. Shangguan, and W. N. Fu, "Finite element analysis of 1 MW high speed wound-rotor synchronous machine," *IEEE Trans. Magn.*, vol. 48, no. 11, pp. 4650–4653, Nov. 2012.

[12] O. Laldin, S. D. Sudhoff, and S. Pekarek, "An analytical design model for wound rotor synchronous machines," *IEEE Trans. Energy Convers.*, vol. 30, no. 4, pp. 1299–1309, Dec. 2015.

[13] W. Chai, W. Zhao, and B. I. Kwon, "Optimal design of wound field synchronous reluctance machines to improve torque by increasing the salieny ratio," *IEEE Trans. Magn.*, vol. 53, no. 11, Nov. 2017, Art. no. 8206604.

[14] A. D. Gioia *et al.*, "Design and demonstration of a wound field synchronous machine for electric vehicle traction with brushless capacitive field excitation," *IEEE Trans. Ind. Appl.*, vol. 54, no. 2, pp. 1390–1403, Mar./Apr. 2018.

[15] G. Jawad, Q. Ali, T. A. Lipo, and B. I. Kwon, "Novel brushless wound rotor synchronous machine with zero-sequence third-harmonic field excitation," *IEEE Trans. Magn.*, vol. 52, no. 7, Jul. 2016, Art. no. 8106104.

[16] B. H. Lee, "Design and optimal efficiency control of wound rotor synchronous machine for EV," Ph.D. Thesis, Automotive Eng., Hanyang Univ., South Korea, Feb. 2013.

[17] S. I. Park and K. C. Kim, "Torque ripple reduction method with asymmetric pole for wound-field synchronous motor," *IEEE Trans. Magn.*, vol. 51, no. 3, Mar. 2015, Art. no. 8102504.

[18] S. H. Do, B. H. Lee, H. Y. Lee, and J. P. Hong, "Torque ripple reduction of wound rotor synchronous motor using rotor slits," in *Proc. IEEE Int. Conf. Elect. Mach. Syst.*, Oct. 2012, pp. 1–4.

[19] S. W. Hwang, J. H. Sim, J. P. Hong, J. Y. Lee, and J. M. Kim, "Torque improvement of wound field synchronous motor for electric vehicle by PM-assist," in *Proc. IEEE Energy Convers. Congr. Expo.*, Sep. 2016, pp. 1–6.

[20] G. Tajima, T. Kosaka, N. Matsui, K. Tonogi, N. Monishima, and T. Yoshida, "Operation evaluations in high speed range of wound field synchronous motor drive integrated with ZSI," in *Proc. IEEE Int. Conf. Mechatronics*, Apr. 2015, pp. 685–690.

[21] G. Tajima, T. Kosaka, and N. Matsui, "Experimental studies on drive performances of wound field synchronous motor drive integrated with ZSI," in *Proc. IEEE Appl. Power Electron. Conf. Expo.*, May 2015, pp. 26269.

[22] A. K. Jain and V. T. Ranganathan, "Hybrid LCI/VSI power circuit—A universal high-power converter solution for wound field synchronous motor drives," *IEEE Trans. Ind. Electron.*, vol. 58, no. 9, pp. 4057–4068, Sep. 2011.

Myung-Seop Lim received the bachelor's degree in mechanical engineering from Hanyang University, Seoul, South Korea, in 2012. He received the master's and Ph.D. degrees in automotive engineering from the Same University, in 2014 and 2017, respectively.

From 2017 to 2018, he was a Research Engineer in Hyundai Mobis, Yongin, South Korea. Since 2018, he has been with Yeungnam University, Daegu, South Korea, where he is currently an Assistant Professor. His research interests include electromagnetic field analysis and electric machinery for mechatronics systems such as automotive and robot applications.

Jung-Pyo Hong (SM'97) received the Ph.D. degree in electrical engineering from Hanyang University, South Korea, in 1995.

From 1996 to 2006, he was a Professor at Changwon National University, Changwon, South Korea. Since 2006, he has been working as a Professor in the Hanyang University, South Korea. His research interests are the design of electric machines, optimization, and numerical analysis of electromechanics.